ECL sensor for selective determination of citrate ion as prostate cancer biomarker using polymer of intrinsic microporosity-1 nanoparticles/nitrogen doped carbon quantum dots

Hosein Afshary [1], Mandana Amiri [1*], Frank Marken [2], Neil B. McKeown [3], Mahdi Amiri [4]

[1] *Department of Chemistry, University of Mohaghegh Ardebil, Ardabil, 59166-11367, Iran*

[2] *Department of Chemistry, University of Bath, Bath BA2 7AY, UK*

[3] *School of Chemistry, University of Edinburgh, David Brewster Road, Edinburgh, EH9 3FJ, UK*

[4] *Imam Hossein Hospital, Social Security Organization, Zanjan Branch, Zanjan, Iran*

Abstract

Urine citrate analysis is relevant in the screening and monitoring of patients with prostate cancer and calcium nephrolithiasis. A sensitive, fast, easy, and low-maintenance electrochemiluminescence (ECL) method with conductivity detection for the analysis of urine citrate is developed and validated by employing polymer of intrinsic microporosity-1 nanoparticles/nitrogen doped carbon quantum dots (nanoPIM-1/N-CQDs). Using the optimum conditions, the sensor was applied for ECL experiments in the presence of different concentrations of citrate ion. The ECL signals were quenched gradually by increasing of the citrate concentration. The linear range of relationship between logarithm of citrate concentration and ΔECL (ECL of blank – ECL of sample) was obtained between 1.0×10^{-7} M and 5.0×10^{-4} M. Limit of detection (LOD) was calculated to be 2.2×10^{-8} M (S/N = 3). The sensor was successfully applied in real samples such as human serum and patient urine.

Keywords: Citrate, Prostate cancer biomarker, Electrochemiluminescence, Carbon dots, PIM-1

[*] Corresponding author. e-mail: mandanaamiri@uma.ac.ir (Tel: +98-45-31502500, Fax: +98-45-33514703)

1. Introduction

Citrate is one of the most important anions due to its vital role in the Krebs cycle, which plays the essential roles in metabolism of aerobic organisms. Measurements of citrate can lead to a better understanding of certain pathological state, for instance, the reduction of citrate in urine associated with kidney dysfunction and prostate cancer. Citrate levels existing in the human serum have concentrations ranging from 0.06 to 0.14 mM. While, they average 25.4 to 28.9 mM in seminal fluid samples among healthy males. However, these levels are so much lower for the people diagnosed with prostate cancer (1). To date, conventional methods have been used for citrate detection include ion chromatography (2), electrochemistry (3), colorimetry (4) and fluorescence (5). However, these methods usually involve specialized and expensive equipment, complicated sample pretreatment and time consuming. Therefore, the development of simple, fast and selective methods for citrate detection is of great significance.

Today sensing based on ECL technique is widely used in various areas because of its tangible benefits in comparison with other analytical methods. In ECL, combination of light and current signals, leads to low background noise, high selectivity and sensitivity, and cheap instrumental determinations in environment, food, and health areas. Emitting materials, that sometimes are called *electrochemiluminophores*, are the most important components of the ECL systems. Therefore, many studies are performed to find and introduce the new types of luminophores due to the need for firstly replacing with the traditional expensive or toxic ones like $Ru(bpy)_3^{2+}$ and secondly improving sensitivity and selectivity for relevant analytes (6-10).

Carbon quantum dots (CQDs) are relatively new kind of carbon materials (discovered in 2004) with unique features including low toxicity, low cost, and with useful physicochemical properties such as electrochemiluminescence. In many cases, especially when doped with heteroatoms, CQDs show enough ECL emission to be applicable as analytical electrochemiluminophores (11-15). Many ECL sensors based on CQDs are studied and developed for determination of different analytes starting from simple ions, like heavy metals, to human body complex materials and disease biomarkers (16, 17). Nitrogen doped carbon quantum dots (N-CQDs) are used in ECL sensors because of an intense cathodic and anodic ECL signal in comparison to emission from pristine CQDs (18-20). Doping of nitrogen is performed using nitrogen-containing precursors.

This results not only in doping of N atom into the structure of CQDs, but also in the formation of N-containing functional groups on the surface of CQDs that leads to more water-soluble and electrochemically active CQDs. In consequence, depending on the precursors and synthesis method (the amount and kind of doping/functional groups) in CQDs could have ECL quenching (or enhancing) properties in the presence of target analytes. For example, synthesizing from urea, citric acid and dimethylformamide precursors by solvothermal method resulted to N-CQDs that showed cathodic ECL and had selectively quenching responses to ceftazidime (CFZ) (21). On the other hand, in other studies, synthesizing CQDs from hydrazine hydrate, citric acid and dimethylformamide using the same methodology, resulted in N-doped carbon dots (HNCDs) that could be used for detection of cell-secreted hydrogen peroxide by anodic ECL (18). N-CQDs synthesized by hydrothermal methods using glucosamine as the carbon and nitrogen source also were used for determination of Cu^{2+} ions. Here, the ECL strength of the N-CQDs/$K_2S_2O_8$ system was increased with increasing of the Cu^{2+} ion concentration (22). Practically, trial and error methods are usually applied to find the appropriate analyte that newly synthesized CQDs are responsive to. Another strategy is based on using an intermediate probe materials, like polymer nanospheres, that interact simultaneously with both analyte and luminophore (CQDs) to be sensitive to analyte producing relevant signal (23, 24).

Previously, it was reported that conversion of bulk Polymer of Intrinsic Microporosity-1 (PIM-1) into nanoparticles can lead to ECL properties (25). PIM-1 has ion and molecule selective properties because of a rigid molecular pore structure for sensing (26, 27). Therefore, it is suggested that PIM-1 nanoparticles could be used for enhancing of both ECL of CQDs and introducing selectivity to target analytes.

In this work, a bi-layer of PIM-1 nanoparticle/ N-CQDs was prepared and used for citrate determination. Cathodic linear sweep voltammetry (-0.5 to -2.2 V vs. Ag/AgCl) was used to study the ECL of sensors for determination of citrate ions. The prepared bi-layer luminophores on the electrode showed very selective and sensitive ECL signal quenching in the presence of citrate ions in human serum and in patients urine samples. The linear range was between 1.0×10^{-7} and 5.0×10^{-4} M and reached to the detection limit of 2.2×10^{-8} M. This linearity is very compatible with the normal amount of citrate ion in healthy male serum (at least 6×10^{-5} M) and its maximum amount

in urine of men diagnosed with prostate cancer (2 mM) (28, 29). However different methods have been used to determine the citrate ion in human body fluids but electrochemiluminescence (ECL) has not been reported so far (30-32). Therefore, the sensor that will be described in this work could be applied for fast screening of citrate levels in human biological fluids, especially in urine, for diagnosing of prostate cancer in early stages.

2. Experimental

2.1. Reagents and Chemicals

Chloroform, dimethylformamide (DMF), methanol, acetic acid (CH_3COOH), phosphoric acid (H_3PO_4), citric acid, ascorbic acid, uric acid, urea, glucose, potassium oxalate, potassium persulphate ($K_2S_2O_8$), ammonium chloride, dipotassium hydrogen phosphate (K_2HPO_4), potassium dihydrogen phosphate (KH_2PO_4), potassium acetate (CH_3COOK), potassium hydroxide (KOH), potassium chloride (KCl), potassium citrate, and boric acid (H_3BO_3) were purchased from Merck. As these chemicals were of analytical grade, they were used without any further purification. Powder form of PIM-1 that was synthesized previously (33, 34). A solution of synthesized and well characterized N-CQDs from our previous study was used (21). Deionized water was used as rinsing agent and solvent for preparation of all buffer solutions. Human serum was kindly provided by Iranian Blood Transfusion Organization (IBTO) Ardabil, Iran. Urine sample of a patient diagnosed with prostate cancer was obtained from local hospital, Zanjan, Iran.

2.2. Apparatus

A μStat ECL potentiostat instrument (DropSens, Spain) combined with a home-made three electrode cell system and a dark box were employed as described in our previous study (21). Morphology and size distribution of PIM-1 nanoparticles were determined by field emission scanning electron microscopy (FESEM) images using a TESCAN MIRA3 LMH FE-SEM instrument. Photoluminescence (PL) studies were performed by fluorescence spectrophotometer (CARY, Varian). A Shimadzu IR Affinity spectrophotometer (Japan) was used for Fourier transform infrared (FTIR) spectroscopy. For preventing the observation of the water peak in FTIR spectra, bulk PIM-1/chloroform solution was mixed with KBr powder and after drying at 110 ^oC for 60 min, used for preparation of pellets. Dynamic light scattering (DLS) curves and zeta potentials were obtained using a Horiba nanoparticle analyzer SZ-100.

2.3.Carbon quantum dots synthesis

A solvothermal method was used for the preparation of nitrogen-doped carbon quantum dots (N-CQDs) based on literature methods [12-14, 21]. Citric acid (CA), urea and dimethylformamide (DMF) were used as carbon source, nitrogen source and solvent, respectively. 2 g citric acid and 4 g urea were dissolved in 20 mL of DMF and stirred to obtain a transparent solution. Then the solution was transferred into a 25 mL Teflon-lined stainless-steel reactor and the sealed reactor was put into an oven and held at 160 °C for 5 h. The resulting a red-brown solution was cooled down to room temperature and centrifuged at 4000 rpm for 15 min to remove precipitates. The obtained supernatant was dialyzed for 3 days using a 2000 Da dialysis bag in deionized water under magnetic stirring. The dialyzing water was changed every 12 h. The dark grey solution of N-CQD was taken from the dialysis bag and stored at 4 ^{0}C for further application [21].

2.4. Preparation of PIM-1 nanoparticles

The re-precipitation method was used for synthesis of the PIM-1 nanoparticles according to a previous study with some adjustments (25). 4 mL of PIM-1/chloroform solution (1 mg mL^{-1}) was added dropwise into 40 mL of methanol under vigorous stirring at room temperature. A yellow opaque mixture was obtained and stirred for 12 h. Centrifugation for 30 min at 4000 rpm was used for separation of nanoparticles. The product was then re-dispersed in 1 mL of methanol by ultra-sonication for 30 min and stored at 4 ^{0}C.

2.5. Fabrication of the modified electrode

The glassy carbon electrode (GCE, diameter = 3 mm) was wet-polished firstly with 0.3 and then with 0.05-micron alumina powder. After rinsing with deionized water, the electrode was dried under airflow and 5 μL of 0.4 mg mL^{-1} N-CQDs solution was drop-cast onto the electrode. N-CQDs formed a film on the electrode surface after placing it in an oven at 65 °C for 10 min. After that, 5 μL of 1.3 mg mL^{-1} methanolic suspension of PIM-1 nanoparticles was drop-cast onto the N-CQDs film. The drying step was repeated and then the modified electrode was equilibrated for 10 min at room temperature in the dark before being using in experiments (**Scheme 1**).

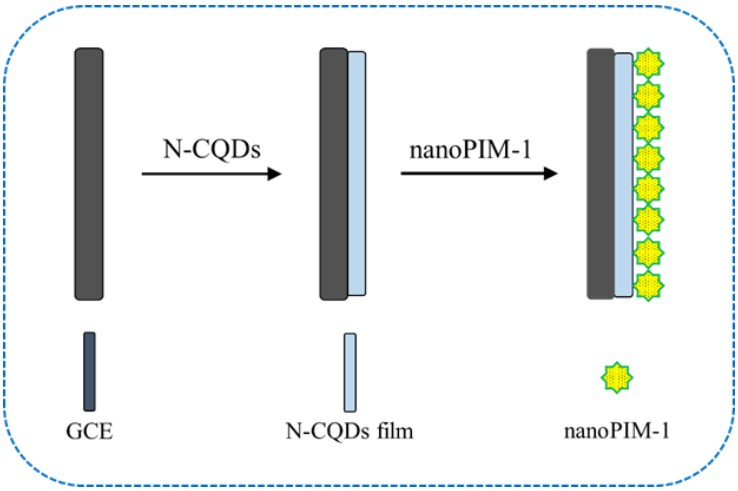

Scheme 1. Schematically illustration of preparation of the sensor

2.6. Preparation of serum and urine samples

For the preparation of serum samples, 5 mL of human serum was mixed with 20 mL of methanol, sonicated for 5 min for precipitating of proteins, and centrifuged for 15 min (4000 rpm). After removing of the floating fats, the supernatant was diluted with PBS solution (pH = 7) to a final volume of 50 mL and used for ECL tests. Spiking of citrate in serum sample before and after removing protein was tested and there was no significant difference between results.

5 mL of urine samples was heated in a water bath at 70 °C for 15 min, centrifuged for 15 min at 4000 rpm and the clear supernatant was diluted with PBS solution (pH = 7) to a final volume of 50 mL and used for tests.

2.7. ECL experiments

Cathodic ECL studies were performed by applying cyclic voltammetry (CV) using Ag/AgCl (sat. KCl) reference electrode, platinum rod as counter electrode and a modified or bare glassy carbon electrode (GCE) as working electrode in a 25 mL ECL cell. Optimum conditions for measurements were obtained by studying the effect of solutions pH, N-CQDs and nano-PIM-1 amounts on the electrode, the co-reactant ($K_2S_2O_8$) concentration, and the scan rate.

3. Results and discussion

3.1. Characterization

The N-CQDs were synthesized according to previous reports with a small modification (35). The product was characterized using different techniques; the results are described by details in our previous work (21). FESEM images of nano-PIM-1 show the morphology of drop cast suspension on a glass substrate (**Fig. 1A**). Using image analyzer software, spherical shapes with well-defined size distribution and average diameter of 19.7 nm of nanoparticles were observed. Zeta potentials of nano-PIM-1 and N-CQDs are shown in **Fig. 1B**. Low negative zeta potential of nano-PIM-1 (-4.5 mV) indicate a weak negative charge of the slightly hydrophobic particles (36). It may some aggregations during drying with nano-PIM-1 layer deposition onto N-CQDs, prevent the loss/erosion of highly soluble and negatively charged CQDs (zeta potential = -32.8 mV) during the analysis. This could improve the stability of the sensor. It is noteworthy that as both zeta potentials were negative. There were no significant electrostatic interactions between N-CQDs and nano-PIM-1 particles. However, hydrophobic interactions are possible and could contribute to quenching or enhancing the ECL properties (37).

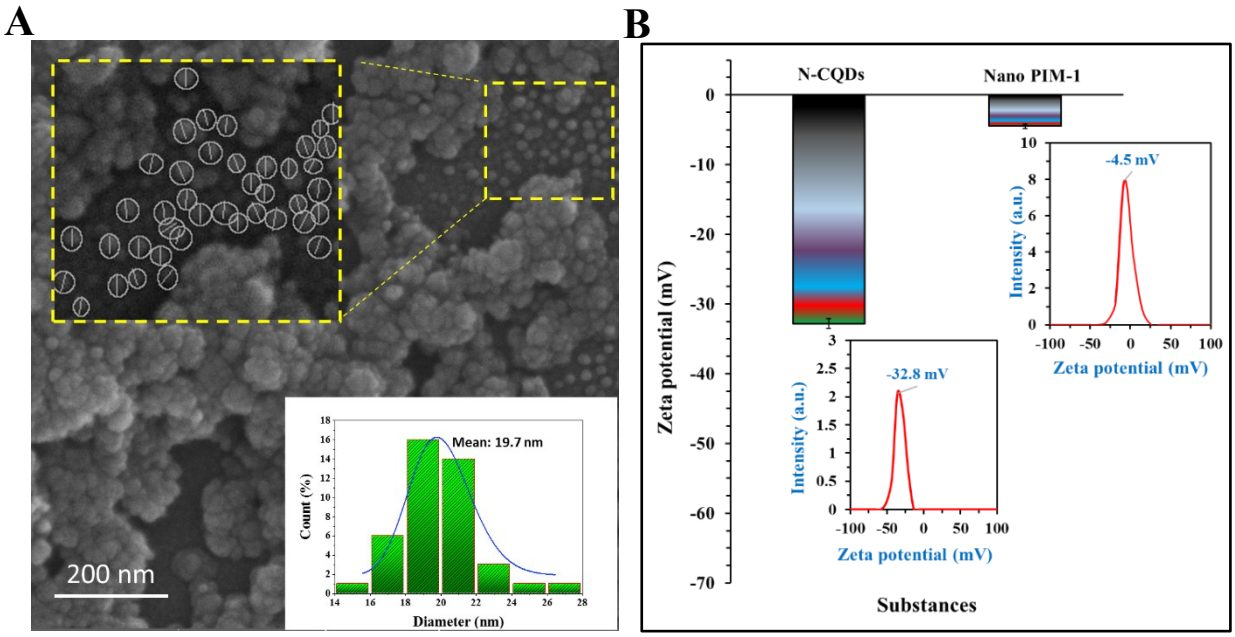

Fig. 1. FESEM and size distribution of nano-PIM-1 (A), zeta potentials of N-CQDs and nano-PIM-1 (B).

FTIR spectra of PIM-1 confirm the presence of −C≡N (2242 cm^{-1}), C−O−C (1738 cm^{-1}), C=C (1600 cm^{-1}), and C−H (1460 cm^{-1}) bonds in the polymer structure (**Fig. 2A**) (38, 39). Optical properties of synthesized nano-PIM-1 were studied by PL spectroscopy. **Fig. 2B** illustrates the survey scan of excitation wavelengths for both bulk and nanoparticle forms of the polymer. As shown, the emissions of nano-PIM-1 are slightly shifted in comparison with the bulk signal. For nano-PIM-1, a new emission also is seen at higher wavelengths. As emission wavelengths of bulk polymer were not changed with different excitation wavelengths (**Fig. 2C**), nanoparticles showed completely different property of so-called excitation-dependent emission (**Fig. 2D** and inset). As ECL and PL are related to each other in most cases, especially in the case of nanostructures, these results could be related to the ECL of the nano-PIM-1 in contrast to the bulk PIM-1.

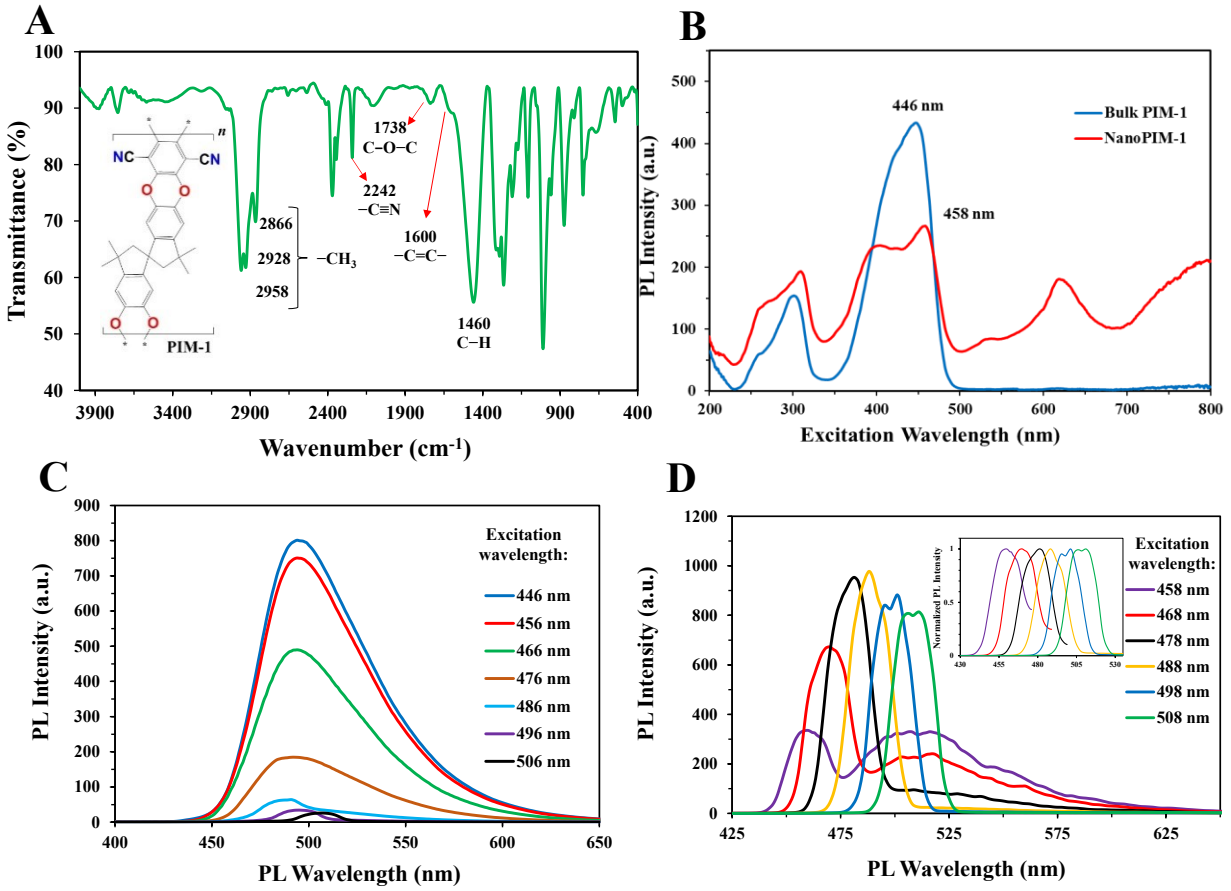

Fig. 2. FTIR and chemical structure of PIM-1 (A), PL survey spectrum of bulk and nanoPIM-1 (B), PL at different excitation wavelengths for bulk (C) and nanoPIM-1 (D).

3.2. ECL properties of nano-PIM-1 and nano-PIM-1/N-CQDs

Cathodic ECL responses of bulk PIM-1, nano-PIM-1, N-CQDs and nano-PIM-1/N-CQDs in the presence of $K_2S_2O_8$ co-reactant are shown in **Fig. 3A**. Curves clearly show that although in the case of bulk PIM-1 there is no ECL signal, for nano-PIM-1 a significant ECL peak is present at a potential of about -1.7 V vs. Ag/AgCl. In the case of layered nano-PIM-1/N-CQDs, the ECL signal is considerably enhanced because of the synergic effect of nano-PIM-1 on N-CQDs. ECL stability of the layered luminophore was studied and the result showed that the ECL sensor has almost invariable/stable signals in several continues experiments (**Fig. 3B**). By comparing the ECL curves of the N-CQDs and nano-PIM-1 (see **Fig. 3A**), it can be concluded that there are different mechanisms of ECL for each one from the different excited state energy levels (see the arrow direction and peak potentials) (40). Proposed ECL mechanism for nano-PIM-1 film on GCE is illustrated in **Fig. 3C**. It was shown earlier that surface functional groups of nano-PIM-1 play a key role in reagentless ECL (25). Here, because of the application of co-reactant and cathodic current, it is proposed that radical species were created on the nano-PIM-1 surface to form the nano-PIM-1$^{\bullet-}$ intermediate. These particles may then react with $SO_4^{\bullet-}$ radicals to form the excited states (nano-PIM-1*) and finally relaxation leads to ECL emission. The proposed mechanism for enhanced ECL of nano-PIM-1/N-CQDs is also shown in **Fig. 3D**. As it is schematically explained, simultaneous ECL of N-CQDs and nano-PIM-1 produce a total enhanced ECL signal. It is better to mention that ECL mechanism of N-CQDs are well-known (15, 16, 41) and here this synergic effect comes from the similar ECL mechanisms of both luminophores that take place in the presence of persulphate coreactant at the vicinity of the cathode. Similar ECL signal amplifications were also reported before (42, 43).

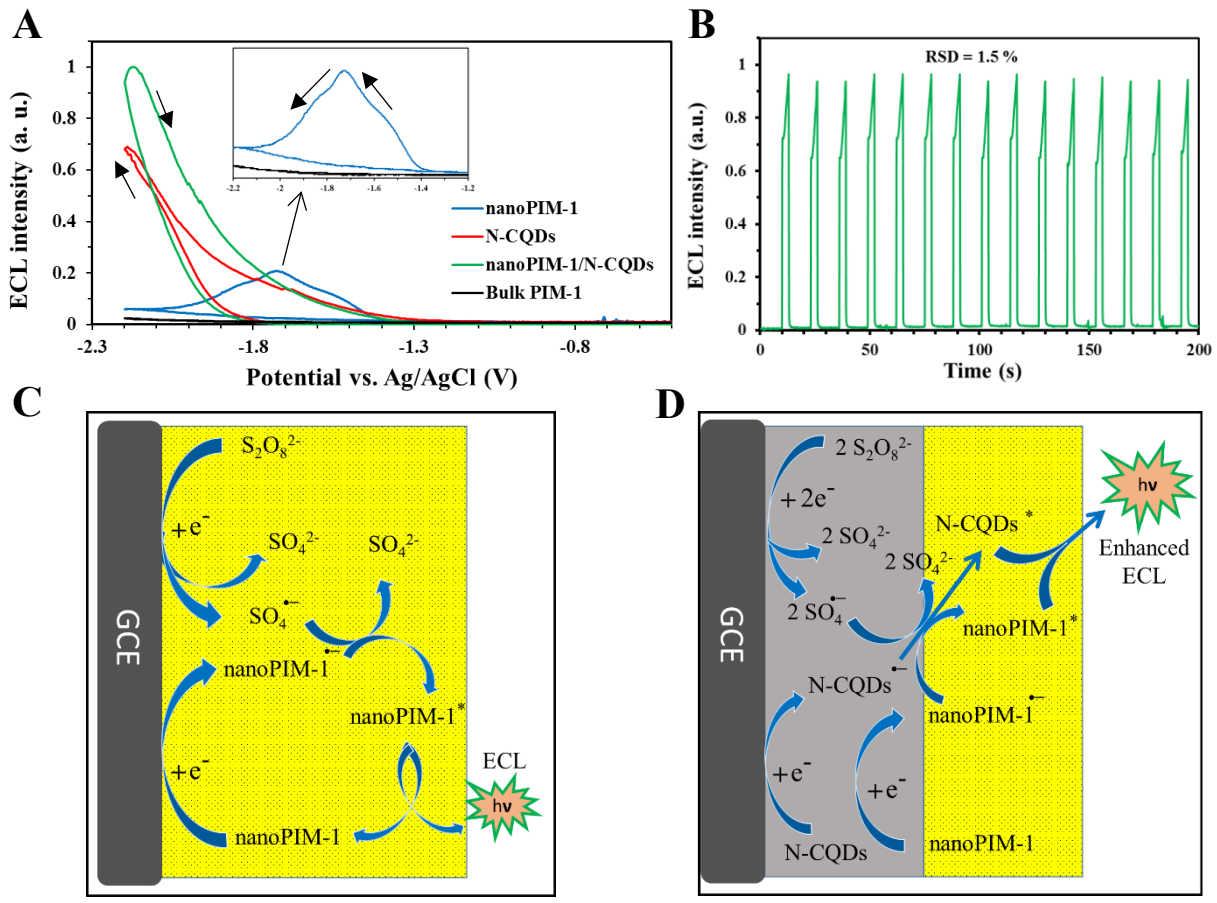

Fig. 3. ECL curves of bulk PIM-1, nano-PIM-1, N-CQDs and nano-PIM-1/N-CQDs in 0.1 M PBS $K_2S_2O_8$ 0.1 M at pH=7 (A), ECL stability curves of nano-PIM-1/N-CQDs (B), proposed ECL mechanism of nano-PIM-1 film on glassy carbon electrode (C), and proposed ECL mechanism of layered film of nano-PIM-1/N-CQDs on glassy carbon electrode (D).

3.3. Optimized ECL conditions for prepared sensor

Three different conditions of luminophore settlement on the electrode including (i) bilayer of nano-PIM-1/N-CQDs/GCE, (i) bilayer of N-CQDs/nano-PIM-1/GCE and (iii) single layer of composite CQDs-nano-PIM-1 composite/GCE were tested and optimized. ECL results show that the bilayer with the order of nano-PIM-1/N-CQDs/GCE provides the best ECL signal and the highest sensitivity to the citrate ion (**Fig. 4A inset**). Therefore, this was used for all further experiments. Other experimental conditions that are very effective to ECL intensity including pH of cell solution, nano-PIM-1 and N-CQD solution concentrations (used for drop casting on the electrode), potential scan rate of CV, and co-reactant concentration were optimized. As shown in **Fig. 4A** and

Fig. 4B and **Fig. 4B inset**, pH = 7, nano-PIM-1 concentration of 1.33 mg mL^{-1} and N-CQDs concentration of 0.43 mg mL^{-1} were the best conditions and selected for all further experiments. **Fig. 4C** shows that the ECL intensity of the sensor was decreased by increasing of the scan rate. This is opposite to current that usually shows direct relationship with scan rate in CV, and shows that at slow scan rates, ECL reactions have enough time to occur. A scan rate of 0.05 V s^{-1} was selected for experiments. **Fig.4D** illustrates that by increasing the $K_2S_2O_8$ concentration, ECL increases until about 0.1 M. This is because the solubility of $K_2S_2O_8$ in 0.1 M buffer solution is limited and reaches to saturation. Therefore, 0.1 M was selected as optimum concentration of persulphate (co-reactant).

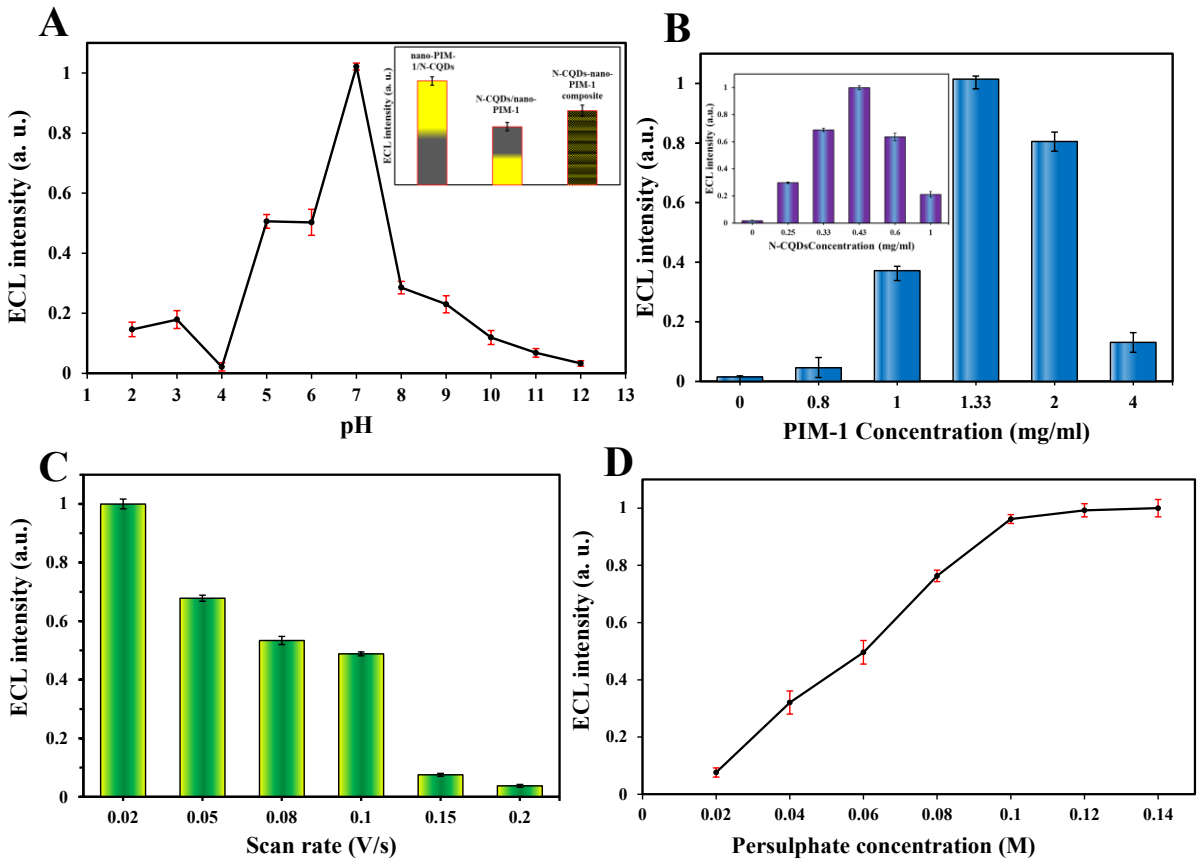

Fig. 4. ECL optimum amounts in different conditions of pH (A), luminophores positions (A inset) nano-PIM-1 and N-CQDs solutions concentrations (B and inset), scan rate (C) and $K_2S_2O_8$ concentration (D).

3.4. Analytical performance of the sensor for detection of citrate ion

Using the optimum conditions, the sensor was applied for ECL experiments in the presence of different concentrations of citrate ions. As shown in **Fig. 5A**,

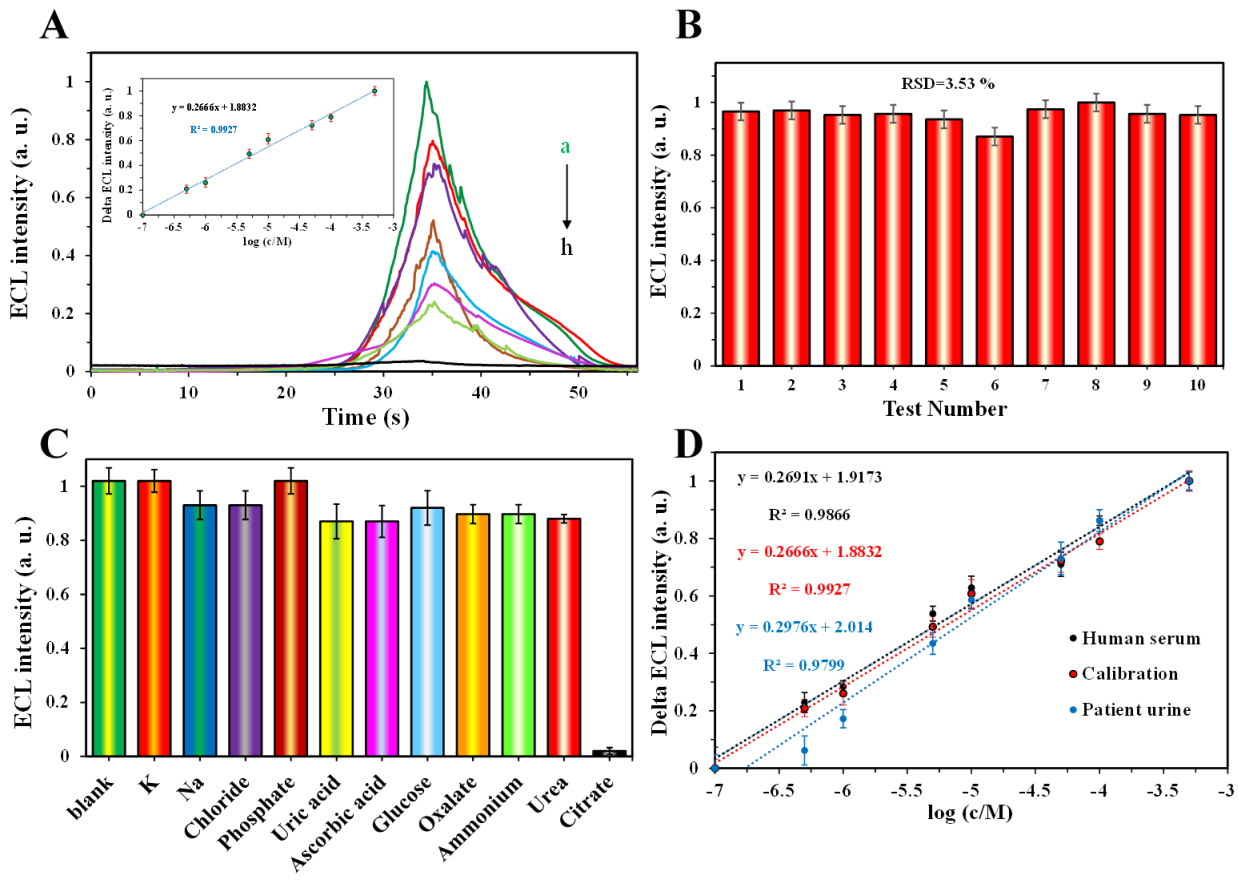

Fig. 5. ECL intensity versus time curves of sensor for different concentration of citrate (A): a) 10^{-7} M, b) 5×10^{-7} M, c) 10^{-6} M, d) 5×10^{-6} M, e) 10^{-5} M, f) 5×10^{-5} M, g) 10^{-4} M, h) 5×10^{-4} M; calibration curve (A inset), reproducibility (B), selectivity (C) and real sample analyses (D).

ECL signals were quenched gradually by increasing of the citrate concentration. Presence of nano-PIM-1 and N-CQDs together resulted higher signals and higher sensitivity, which leads to citrate lower concentration determination compare to employing N-CQDs alone. PIM-1 as a microporous material (pore size typically 1 nm) was used as selective gas separation membrane in early studies (44, 45). The compatibility of the pore sizes of the membrane and radius of the gas molecules was reported as one of the important factors for the selective permeation and separation. On the other hand, physicochemical behaviour of PIM-1 micropores in aqueous solution leading to its size-

sieving effect has been used in electrochemical applications (46). It could be proposed that the selectivity of the sensor is related to citrate ion size and its interaction with micropores that lead to quenching of both nano-PIM-1 and N-CQDs ECL signals.

An acceptable linear range of relationship between logarithm of citrate concentration and delta ECL (ECL of blank – ECL of sample) was obtained between 10^{-7} M and 5×10^{-4} M (**Fig. 5A** inset). This linear range meets the analytical challenge for citrate concentration detection in human serum and in urine and therefore the sensor could be applied directly to analysis of these real samples (28, 29). The regression equation ($R^2 = 0.992$) was used for calculation of citrate concentration in real samples. Limit of detection (LOD) and limit of quantification (LOQ) were calculated to be 2.22×10^{-8} M and 2.23×10^{-8} M respectively (S/N = 3). Analytical parameters for the proposed ECL sensor were compared with other sensing methods in the literature and results are shown in **Table 1**.

Table 1. Comparison of sensing parameters of this work with other methods for determination of citrate.

Method	Real sample	Linear range (M)	LOD (M)	Reference
Colorimetric	Human urine	$5\times10^{-7} - 10^{-3}$	10^{-7}	(28)
Colorimetric	Fruit juice	$1.67\times10^{-7} - 1.22\times10^{-5}$	2.0×10^{-8}	(4)
Fluorescence	Artificial urine	$10^{-7} - 5\times10^{-6}$	10^{-7}	(31)
Fluorescence	Artificial urine and bovine serum	$10^{-7} - 4\times10^{-5}$	1.8×10^{-7}	(32)
Fluorescence	Human urine	$5\times10^{-7} - 10^{-5}$	1.23×10^{-8}	(47)
Colorimetric and fluorescence	Human urine	$10^{-7} - 5\times10^{-5}$	2.5×10^{-8}	(48)
Colorimetric and fluorescence	Fruit juices and human urine	$5.3\times10^{-8} - 8.3\times10^{-7}$	6×10^{-9}	(49)
Capillary Zone Electrophoresis	Blood Plasma	-	$\sim10^{-4}$	(50)
Nuclear magnetic resonance spectroscopy	Human serum and plasma	$7.4\times10^{-5} - 2.3\times10^{-4}$	4×10^{-5}	(51)
Ion-Chromatography	Human urine	$8\times10^{-5} - 10^{-2}$	3×10^{-5}	(2)
Electrochemical	Human urine	$10^{-8} - 10^{-1}$	1.7×10^{-9}	(29)
Electrochemical	Drug	$8\times10^{-7} - 10^{-2}$	5×10^{-7}	(3)
Electrochemiluminescence	**Patient urine and human serum**	$\mathbf{10^{-7} - 5\times10^{-4}}$	$\mathbf{2.22\times10^{-8}}$	**This work**

3.5. Real sample analysis

The capability of the sensor for determination of citrate ion in real samples was tested by analyzing the healthy human serum and urine from a man diagnosed with prostate cancer. Standard addition method using dilute real samples was applied for this aim. Resulted curves are depicted in **Fig. 5D** comparing with the calibration curve. The results show that recoveries for serum and urine samples were 100.93 % and 111.62 %, respectively. Using calibration curve, the amount of citrate ion in the urine of the man diagnosed with prostate cancer was calculated to be 3.14×10^{-4} M, which is consistent with extrapolating of standard addition method. Citrate amount in urine was less than minimum amount of normal citrate level (2×10^{-3} M) supporting the diagnosis (28).

4. Conclusion

It has been shown that both N-CQDs and nano-PIM-1 particles show ECL activity. A layer of N-CQDs coated with nano-PIM-1 shows significantly improved ECL. ECL signals were quenched gradually by increasing of the citrate concentration. Presence of nano-PIM-1 and N-CQDs together resulted higher signals and higher sensitivity, which leads to citrate lower concentration determination compare to employing N-CQDs alone. As citrate is one of the most important anions in biological fluids that can be used as biomarker in prostate cancer. The presented sensor was applied to human serum and patient urine to determine citrate successfully.

Author contribution: All authors contributed to the study conception and design. The first draft of the manuscript was written by MA and HA, and all authors commented on previous versions of the manuscript. All authors read and approved the final manuscript.

Acknowledgment

The authors gratefully acknowledge the support of this work by the University of Mohaghegh Ardabili Research Council, Ardabil, Iran (grant number 3051234502).

Declarations

- Conflicts of interests/Competing interests: The authors declare no conflict of/competing interests.

- Source of biological material: Serum and urine samples were collected from anonymous patients and control donors with informed consent (the origin of the samples are from Imam Hossein Hospital, Social Security Organization, Zanjan Branch, Zanjan, Iran).

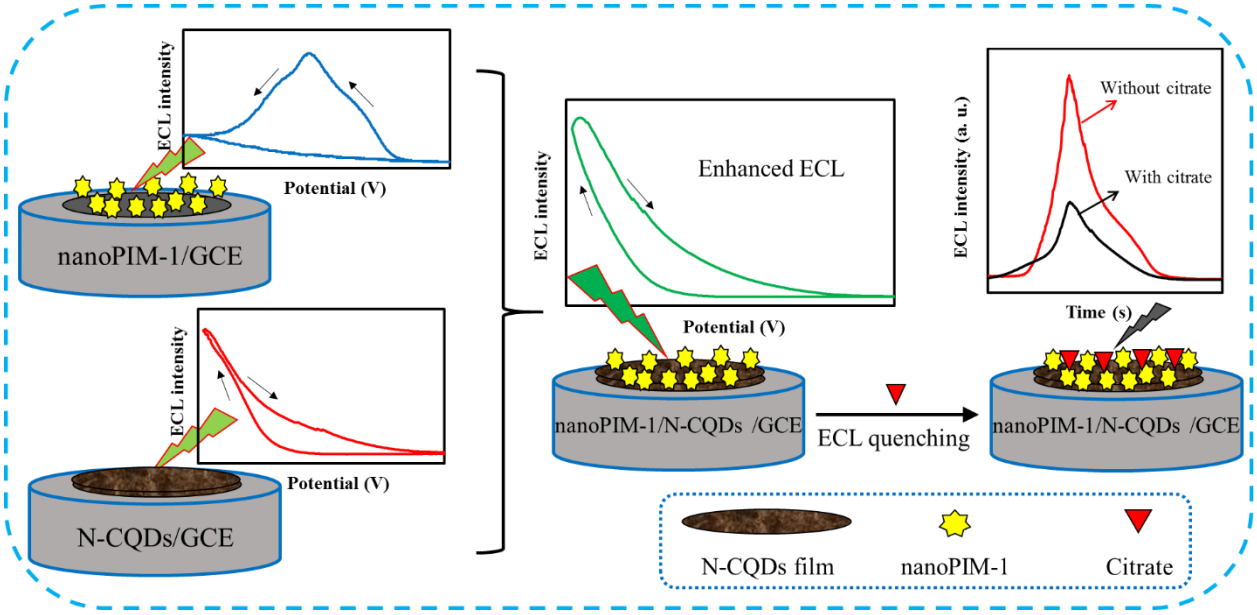

Graphical abstract

References

1. Zhao Y, Shen Y, Wen Y, Campbell RE. High-Performance Intensiometric Direct- and Inverse-Response Genetically Encoded Biosensors for Citrate. ACS Central Science. 2020;6(8):1441-50.
2. Petrarulo M, Leporati M, Pullara F, Frattini M, Nannavecchia V, Marangella M, et al. Sensitive Ion-Chromatographic Determination of Citric Acid in Urine. Separations. 2022;9(6):143.
3. Nooredeen NM, Abd El-Ghaffar MA, Darwish WM, Elshereafy E, Radwan AA, Abbas MN. Graphene oxide with covalently attached zinc monoamino-phthalocyanine coated graphite electrode as a potentiometric platform for citrate sensing in pharmaceutical preparations. Journal of Solid State Electrochemistry. 2015;19(7):2141-54.
4. Tavallali H, Deilamy-Rad G, Parhami A, Hasanli N. An efficient and ultrasensitive rhodamine B-based reversible colorimetric chemosensor for naked-eye recognition of molybdenum and citrate ions in aqueous solution: Sensing behavior and logic operation. Spectrochimica Acta Part A: Molecular and Biomolecular Spectroscopy. 2015;139:253-61.
5. Rajalakshmi K, Nam Y-S, Selvaraj M, Lee Y, Lee K-B. Metal free bioimaging reagent for intracellular citrate in prostate cancer cells using aryl boronate derivative. Sensors and Actuators B: Chemical. 2018;259:90-6.
6. Kerr E, Hayne DJ, Soulsby LC, Bawden JC, Blom SJ, Doeven EH, et al. A redox-mediator pathway for enhanced multi-colour electrochemiluminescence in aqueous solution. Chemical Science. 2022;13(2):469-77.
7. Yang E, Zhang Y, Shen Y. Quantum dots for electrochemiluminescence bioanalysis - A review. Analytica Chimica Acta. 2021:339140.
8. Gu Y, Hu Y, Zhang F, Yi L, Shang Y, Ren D, et al. Electrochemiluminescence sensor based on cyclic peptides-recognition and Au nanoparticles assisted graphitic carbon nitride for glucose determination. Microchimica Acta. 2021;188(5):151.
9. Abdussalam A, Xu G. Recent advances in electrochemiluminescence luminophores. Analytical and bioanalytical chemistry. 2021.
10. Luo L, Liu X, Bi X, Li L, You T. Facile fabrication and application of an innovative self-enhanced luminophore with outstanding electrochemiluminescence properties. Sensors and Actuators A: Physical. 2020;312:112167.
11. Wang L, Liu P, Liu Z, Cao H, Ye S, Zhao K, et al. A dual-potential ratiometric electrochemiluminescence biosensor based on Au@CDs nanoflowers, Au@luminol nanoparticles and an enzyme-free DNA nanomachine for ultrasensitive p53 DNA detection. Sensors and Actuators B: Chemical. 2021;327:128890.
12. Arcudi F, Đorđević L, Rebeccani S, Cacioppo M, Zanut A, Valenti G, et al. Lighting up the Electrochemiluminescence of Carbon Dots through Pre- and Post-Synthetic Design. Advanced Science. 2021;8(13):2100125.
13. Chen X, Liu Y, Ma Q. Recent advances in quantum dot-based electrochemiluminescence sensors. Journal of Materials Chemistry C. 2018;6(5):942-59.
14. Zhang T-T, Zhao H-M, Fan X-F, Chen S, Quan X. Electrochemiluminescence immunosensor for highly sensitive detection of 8-hydroxy-2′-deoxyguanosine based on carbon quantum dot coated Au/SiO2 core–shell nanoparticles. Talanta. 2015;131:379-85.

15. Yang E, Yang H, Ning Z, Fang Y, Chen M, Zheng Y, et al. Construction of Carbon Dots with Wavelength-Tunable Electrochemiluminescence and Enhanced Efficiency. Analytical Chemistry. 2022.
16. Li L, Zhao W, Luo L, Liu X, Bi X, Li J, et al. Electrochemiluminescence of Carbon-based Quantum Dots: Synthesis, Mechanism and Application in Heavy Metal Ions Detection. Electroanalysis. 2022;34(4):608-22.
17. Chen Y, Cao Y, Ma C, Zhu J-J. Carbon-based dots for electrochemiluminescence sensing. Materials Chemistry Frontiers. 2020;4(2):369-85.
18. Chen A, Liang W, Wang H, Zhuo Y, Chai Y, Yuan R. Anodic Electrochemiluminescence of Carbon Dots Promoted by Nitrogen Doping and Application to Rapid Cancer Cell Detection. Analytical Chemistry. 2019.
19. Liu Q, Ma C, Liu X-P, Wei Y-P, Mao C-J, Zhu J-J. A novel electrochemiluminescence biosensor for the detection of microRNAs based on a DNA functionalized nitrogen doped carbon quantum dots as signal enhancers. Biosensors and Bioelectronics. 2017;92:273-9.
20. Xiong C, Liang W, Wang H, Zheng Y, Zhuo Y, Chai Y, et al. In situ electro-polymerization of nitrogen doped carbon dots and their application in an electrochemiluminescence biosensor for the detection of intracellular lead ions. Chemical Communications. 2016;52(32):5589-92.
21. Afshary H, Amiri M, Bezaatpour A, Wark M. Electrochemiluminescence Sensor Based on N-Doped Carbon Quantum Dots for Determination of Ceftazidime in Real Samples. Journal of The Electrochemical Society. 2022;169(2):026523.
22. Li R, Zhu Z, Pan P, Liu J, Zhou B, Liu C, et al. One-step synthesis of nitrogen-doped carbon quantum dots for paper-based electrochemiluminescence detection of Cu2+ ions. Microchemical Journal. 2022;174:107057.
23. Qin D, Jiang X, Mo G, Zheng X, Deng B. Electrochemiluminescence immunoassay of human chorionic gonadotropin using silver carbon quantum dots and functionalized polymer nanospheres. Microchimica Acta. 2020;187(8):482.
24. Qin D, Jiang X, Mo G, Feng J, Yu C, Deng B. A Novel Carbon Quantum Dots Signal Amplification Strategy Coupled with Sandwich Electrochemiluminescence Immunosensor for the Detection of CA15-3 in Human Serum. ACS Sensors. 2019;4(2):504-12.
25. Madrid E, He D, Yang J, Hogan CF, Stringer B, Msayib KJ, et al. Reagentless Electrochemiluminescence from a Nanoparticulate Polymer of Intrinsic Microporosity (PIM-1) Immobilized onto Tin-Doped Indium Oxide. ChemElectroChem. 2016;3(12):2160-4.
26. Marken F, Wang L, Zhao Y, Li Z, Amiri M, Imanzadeh H. Polymers of intrinsic microporosity (PIMs) in sensing and in electroanalysis. Current Opinion in Chemical Engineering. 2022;35:100765.
27. Marken F, Carta M, McKeown NB. Polymers of Intrinsic Microporosity in the Design of Electrochemical Multicomponent and Multiphase Interfaces. Analytical Chemistry. 2020.
28. Abarghoei S, Fakhri N, Borghei YS, Hosseini M, Ganjali MR. A colorimetric paper sensor for citrate as biomarker for early stage detection of prostate cancer based on peroxidase-like activity of cysteine-capped gold nanoclusters. Spectrochimica Acta Part A: Molecular and Biomolecular Spectroscopy. 2019;210:251-9.
29. Azzouzi S, Patra HK, Ben Ali M, Abbas MN, Dridi C, Errachid A, et al. Citrate-selective electrochemical μ-sensor for early stage detection of prostate cancer. Sensors and Actuators B: Chemical. 2016;228:335-46.
30. Shaban SM, Lee JY, Kim D-H. Dual-Surfactant-Capped Ag Nanoparticles as a Highly Selective and Sensitive Colorimetric Sensor for Citrate Detection. ACS Omega. 2020;5(19):10696-703.
31. Liu C, Hang Y, Jiang T, Yang J, Zhang X, Hua J. A light-up fluorescent probe for citrate detection based on bispyridinum amides with aggregation-induced emission feature. Talanta. 2018;178:847-53.

32. Hang Y, Wang J, Jiang T, Lu N, Hua J. Diketopyrrolopyrrole-Based Ratiometric/Turn-on Fluorescent Chemosensors for Citrate Detection in the Near-Infrared Region by an Aggregation-Induced Emission Mechanism. Analytical Chemistry. 2016;88(3):1696-703.
33. Budd PM, McKeown NB, Fritsch D, editors. Polymers of intrinsic microporosity (PIMs): high free volume polymers for membrane applications. Macromolecular Symposia; 2006: Wiley Online Library.
34. Budd PM, Elabas ES, Ghanem BS, Makhseed S, McKeown NB, Msayib KJ, et al. Solution-processed, organophilic membrane derived from a polymer of intrinsic microporosity. Advanced Materials. 2004;16(5):456-9.
35. Su W, Li J, Chen F, Fu L, Ding S, Zhao S, et al. Enhancing Nonradiative Energy Transfer between Nitridized Carbon Quantum Dots and Monolayer WS2. The Journal of Physical Chemistry C. 2019.
36. Desmet C, Valsesia A, Oddo A, Ceccone G, Spampinato V, Rossi F, et al. Characterisation of nanomaterial hydrophobicity using engineered surfaces. Journal of Nanoparticle Research. 2017;19(3):117.
37. Li F, Rui J, Yan Z, Qiu P, Tang X. A highly sensitive dual-read assay using nitrogen-doped carbon dots for the quantitation of uric acid in human serum and urine samples. Microchimica Acta. 2021;188(9):311.
38. Valle M, Martín L, Maestro A, Andrés JM, Pedrosa R. Chiral Bifunctional Thioureas and Squaramides Grafted into Old Polymers of Intrinsic Microporosity for Novel Applications. Polymers. 2019;11(1):13.
39. Liu Y, Zhang J, Tan X. High Performance of PIM-1/ZIF-8 Composite Membranes for O2/N2 Separation. ACS Omega. 2019;4(15):16572-7.
40. Guo W, Ding H, Su B. Electrochemiluminescence of metallated porous organic polymers. Journal of Electroanalytical Chemistry. 2018;818:176-80.
41. Molaei MJ. Principles, mechanisms, and application of carbon quantum dots in sensors: a review. Analytical Methods. 2020.
42. Wen J, Zhou L, Jiang D, Shan X, Wang W, Shiigi H, et al. Ultrasensitive ECL aptasensing of kanamycin based on synergistic promotion strategy using 3,4,9,10-perylenetetracar-boxylic-l-cysteine/Au@HKUST-1. Analytica Chimica Acta. 2021;1180:338780.
43. Han S, Gao Y, Li L, Lu B, Zou Y, Zhang L, et al. Synergistic Enhancement Effects of Carbon Quantum Dots and Au Nanoclusters for Cathodic ECL and Non-enzyme Detections of Glucose. Electroanalysis. 2020;n/a(n/a).
44. Budd PM, McKeown NB, Ghanem BS, Msayib KJ, Fritsch D, Starannikova L, et al. Gas permeation parameters and other physicochemical properties of a polymer of intrinsic microporosity: Polybenzodioxane PIM-1. Journal of Membrane Science. 2008;325(2):851-60.
45. Heuchel M, Fritsch D, Budd PM, McKeown NB, Hofmann D. Atomistic packing model and free volume distribution of a polymer with intrinsic microporosity (PIM-1). Journal of Membrane Science. 2008;318(1):84-99.
46. Wang L, Zhao Y, Fan B, Carta M, Malpass-Evans R, McKeown NB, et al. Polymer of intrinsic microporosity (PIM) films and membranes in electrochemical energy storage and conversion: A mini-review. Electrochemistry Communications. 2020;118:106798.
47. Cheng Q, Liu X, He Y, Ge Y, Zhou J, Song G. Fabrication of Fluorescence Turn-off-on Sensor Based on g-C3N4 Quantum Dots and MgFe Layered Double Hydroxide for the Detection of Citrate. Journal of Fluorescence. 2019;29(3):719-26.
48. Li C-Y, Zhou Y, Li Y-F, Kong X-F, Zou C-X, Weng C. Colorimetric and fluorescent chemosensor for citrate based on a rhodamine and Pb2+ complex in aqueous solution. Analytica Chimica Acta. 2013;774:79-84.
49. Tavallali H, Baezzat M-R, Deilamy-Rad G, Parhami A, Hasanli N. An ultrasensitive and highly selective fluorescent and colorimetric chemosensor for citrate ions based on rhodamine B and its

application as the first molecular security keypad lock based on phosphomolybdic acid and citrate inputs. Journal of Luminescence. 2015;160:328-36.
50. Polyakova EV, Shuvaeva OV, Borisov AS. Determination of Citrate Ions in Blood Plasma by Capillary Zone Electrophoresis. Journal of Analytical Chemistry. 2018;73(9):906-9.
51. Garcia E, Connelly MA, Matyus SP, Otvos JD, Shalaurova I. High-throughput nuclear magnetic resonance measurement of citrate in serum and plasma in the clinical laboratory. Practical Laboratory Medicine. 2021;25:e00213.